

## SYNTHESIS, CHARACTERIZATION, AND PHOTOCATALYTIC EFFICIENCY OF A NEW SMART PdO OXIDE NANOMATERIALS FOR USING IN THE RECYCLING AND SUSTAINABLE WASTEWATER TREATMENT

Moamen S. Refat\*, Hosam A Saad, Adil A. Gobouri, Mohammed Alsawat, Kaouther Belgacem, Badriah M. Majrashi and Abdel Majid A. Adam

Department of Chemistry, College of Science, Taif University, P.O. Box 11099, Taif 21944, Saudi Arabia

(Received August 12, 2020; Revised January 9, 2021; Accepted January 20, 2021)

**ABSTRACT.** Nanostructured PdO materials with promising catalytic properties were successfully synthesized by the controlled thermal decomposition in air of three Pd(II) complexes containing Pd(II) ion, ofloxacin drug and amino acid. The Pd(II) complexes which were used as precursors were [Pd(OFL)(Gly)]Cl, [Pd(OFL)(Ala)]Cl, and [Pd(OFL)<sub>2</sub>]Cl<sub>2</sub>, where Gly is glycine amino acid, Ala is alanine amino acid, and OFL is ofloxacin. Structural and morphological properties of the synthesized PdO materials were obtained using FTIR, XRD, SEM, and EDX techniques. The XRD results confirm the tetragonal structure of PdO. The obtained PdO materials were tested as a catalyst for the heterogeneous degradation of H<sub>2</sub>O<sub>2</sub> solution. The results revealed that PdO could effectively degrade H<sub>2</sub>O<sub>2</sub>.

**KEY WORDS:** PdO, Nanoparticles, Photocatalytic efficiency, Wastewater treatment

### INTRODUCTION

Providing a clean environment that is free of any pollutants, toxic and hazardous or otherwise, is an important concern of scientists world-wide and this goal can be achieved with the help of environmentally friendly chemistry using transition metal oxides. These oxides, like RuO<sub>2</sub>, Co<sub>3</sub>O<sub>4</sub>, TiO<sub>2</sub>, NiO, PdO, MnO<sub>2</sub>, ZnO, In<sub>2</sub>O<sub>3</sub>, SnO<sub>2</sub>, and TiO<sub>2</sub>, possess good semiconductor properties, like a significant band gap, as well as transport and optical properties that utilize transition metal oxides for different advanced photocatalytic applications [1-14]. Many pollutants and toxic and hazardous substances, like textile dyes, pesticides, and pharmaceutical drugs, were removed from environments based on photocatalytic degradation in visible light catalyzed by nanostructured transition metal oxides because the metal oxides, in nano-scale ranges, possess high surface areas and improved reactive sites [15-22]. Palladium oxide (PdO) possesses a band gap value equal to 2.2 eV and it considered a p-type semiconductor [23, 24]. Recently, palladium metal (Pd) and its oxide (PdO) have received special attention and extensive investigation due to their unique properties as catalysts because they possess high catalytic potency at low temperatures and low volatility at high temperatures. They have wide applications [25-39] in methane combustion [25-28], carbon monoxide oxidation [29-32], catalyzing several organic conversions and reactions, like reduction reactions, hydrogenations of unsaturated olefins, and carbon-carbon cross-coupling formation [33-35], ethanol oxidation; it decomposes ethanol through decarbonylation and dehydrogenation, releasing CO and H species and environmental redemption applications when incorporating Pd or PdO with TiO<sub>2</sub>. This incorporation reduced the band gap of TiO<sub>2</sub>. This incorporating material showed extremely high photocatalytic degradation of rhodamine and methylene blue [36-39].

In this work, nanostructured PdO materials were prepared via the controlled thermal decomposition at low temperatures in air of three Pd(II) complexes containing Pd(II) ion,

\*Corresponding author. E-mail: msrefat@yahoo.com; moamen@tu.edu.sa

This work is licensed under the Creative Commons Attribution 4.0 International License

ofloxacin drug, and amino acid, and these materials were analyzed for their structural and morphological properties using the Shimadzu FT-IR spectrophotometer, XRD, SEM, and EDX techniques. The three complexes which were used as precursors were complex **I** ([Pd(OFL)(Gly)]Cl), complex **II** ([Pd(OFL)(Ala)]Cl), and complex **III** ([Pd(OFL)<sub>2</sub>]Cl<sub>2</sub>), where Gly is glycine amino acid, Ala is alanine amino acid, and OFL is ofloxacin. The heterogeneous catalytic degradation of the prepared PdO materials as catalysts toward H<sub>2</sub>O<sub>2</sub> was examined at room temperature in water.

## EXPERIMENTAL

### General

The chemicals were of analytical grades and were bought from BDH (UK) and Sigma-Aldrich (USA) chemical companies. The instruments X'Pert Philips X-ray powder diffractometer and Shimadzu FT-IR spectrophotometer were used to collect the XRD and IR spectra of the PdO materials, respectively. Their XRD spectra were scanned from 2θ of 105° to 20°, where their IR spectra were scanned from wavenumber of 400 cm<sup>-1</sup> to 4000 cm<sup>-1</sup>.

The SEM and EDX profiles for the PdO materials were obtained using the instruments Joel JSM-639OLV scanning electron microscope (SEM) and Noran six 200 energy dispersive X-ray (EDX) analyzer, respectively.

### Synthesis of the PdO materials

Three Pd(II) complexes containing Pd(II) ion, ofloxacin drug, and amino acid (glycine or alanine) were synthesized according to the literature method [40]. These complexes are: **I**: [Pd(OFL)(Gly)]Cl, **II**: [Pd(OFL)(Ala)]Cl and **III**: [Pd(OFL)<sub>2</sub>]Cl<sub>2</sub>.

Complex **I**, [Pd(OFL)(Gly)]Cl was prepared by adding a hot methanolic solution (2 mmol, 40 mL, 0.722 g) of OFL to an aqueous solution (2 mmol, 25 mL, 0.354 g) of PdCl<sub>2</sub> and glycine (2 mmol, 5 mL, 0.150 g). The reaction mixtures were neutralized at pH = 8-9 and then refluxed for 6-7 h at ~70-80 °C. The solution was filtered off and left to slowly evaporate. Then, they were dried in an oven to dispose of the solvent after 6-15 h. Yellow color product was deposited and collected in a glass bottle for the chemical analyses.

Complex **II**, [Pd(OFL)(Ala)]Cl was prepared by adding a hot methanolic solution (2 mmol, 40 mL, 0.722 g) of OFL to an aqueous solution (2 mmol, 25 mL, 0.354 g) of PdCl<sub>2</sub> and alanine (2 mmol, 5 mL, 0.178 g). The reaction mixtures were neutralized at pH = 8-9 and then refluxed for 6-7 h at ~70-80 °C. The solution was filtered off and left to slowly evaporate. Then, it was dried in a drying oven to dispose of the solvent after 6-15 h. Yellowish white color product deposited and was collected in a glass bottle for the chemical analyses.

Complex **III**, [Pd(OFL)<sub>2</sub>]Cl<sub>2</sub> was prepared by adding a hot methanolic solution (4 mmol, 40 mL, 1.445 g) of OFL ligand to an aqueous solution (2 mmol, 15 mL, 0.354 g) of PdCl<sub>2</sub>. The reaction mixture was neutralized at pH = 8-9 and then refluxed for 6-7 h at ~70-80 °C. The colored solution was filtered off and left to slowly evaporate. Afterwards, it was dried in an oven to dispose of the remaining solvent, and yellowish white color products deposited and were collected in a glass bottle for the chemical analyses.

The Gly in these complexes is glycine amino acid, Ala is alanine amino acid, and OFL is ofloxacin drug. The chemical structures of **I**, **II** and **III** are presented in Figure 1. Nanostructured PdO materials were prepared by the controlled thermal decomposition of **I**, **II** and **III** as precursors in air at temperatures of 600 °C for 3 h using electric furnace. The obtained PdO products were ground into fine powder (2-3 mm), and then characterized by the FTIR, XRD, SEM, and EDX methods.

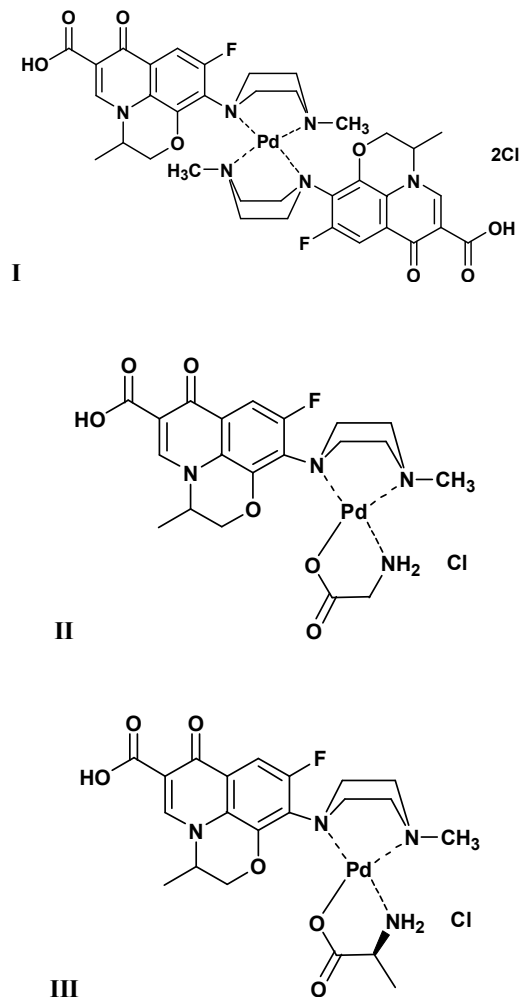


Figure 1. Chemical structures I, II and III.

#### Catalytic experiment

The catalytic decomposition of  $\text{H}_2\text{O}_2$  by the synthetic PdO has been observed by titration of the undecomposed  $\text{H}_2\text{O}_2$  with a standard solution of  $\text{KMnO}_4$ . The PdO (0.02 g) was mixed with 5 mL of  $\text{H}_2\text{O}_2$  (0.01 N) in a conical flask under magnetic stirring at room temperature. The decomposition of  $\text{H}_2\text{O}_2$  was investigated at different times within the range of 10-50 min. Then, a 5-mL aliquot of reaction mixture was titrated with (0.1 N)  $\text{KMnO}_4$  in the presence of an acidic  $\text{H}_2\text{SO}_4$  solution, and the difference in consumed volumes of the  $\text{KMnO}_4$  solution before and after the catalytic decomposition was calculated.

## RESULTS AND DISCUSSION

### *Characterization of the PdO materials*

The PdO materials were generated from the solid-state thermal decomposition of **I**, **II** and **III** at 600 °C. The composition, crystallinity, and surface morphology of the obtained PdO materials were investigated using XRD, SEM, EDX and FTIR methods. Figure 2 a-c depicts the IR spectra of the prepared PdO materials. Generally, metal oxides showed IR absorption bands in the fingerprint region below 1000  $\text{cm}^{-1}$  appeared from inter-atomic vibrations. The prepared PdO materials showed weak bands around 1200  $\text{cm}^{-1}$  and 3000  $\text{cm}^{-1}$ , which may be assigned to the O–H deformation and stretching vibrations, respectively. These bands arise from the water adsorption on the PdO surface. Bands located at 580  $\text{cm}^{-1}$  and 650  $\text{cm}^{-1}$  were attributed to the Pd–O stretching vibrations [41]. Peroxo groups stretching vibrations showed that the absorption band appeared at 1365  $\text{cm}^{-1}$  [42]. Figure 3 a-c represents the XRD patterns of the prepared PdO materials. These materials showed characteristic diffraction peaks at  $2\theta$  values of 71.34° (211), 60.07° (103), 54.71° (112), 42.03° (110), 39.78° (101), and 33.57° (002). These peaks can be indexed to tetragonal PdO (JCPDS Card No. 75–584) [43]. Based on the Debye-Scherrer equation, the average particle size for the PdO materials was estimated to be ~ 40 nm. The XRD spectra of the PdO materials showed some minor peaks, which could be due to the presence of trace of impurities presented in PdO. Figure 4 a-c presents the SEM micrographs of the prepared PdO materials taken with different scales from 1 to 50  $\mu\text{m}$  and various magnifications (1,000x to 20,000x). These micrographs indicate that the particles of PdO were agglomerated with non-defined structural morphology. The non-defined shaped of the particles could be due to the high surface energy of the particles and the strong tendency to form agglomerates.

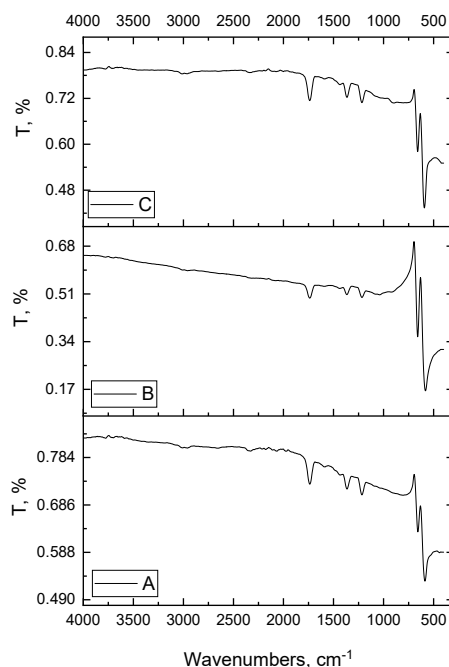


Figure 2. IR spectra of PdO generated from the calcination of **I** (A), **II** (B) and **III** (C) complexes.

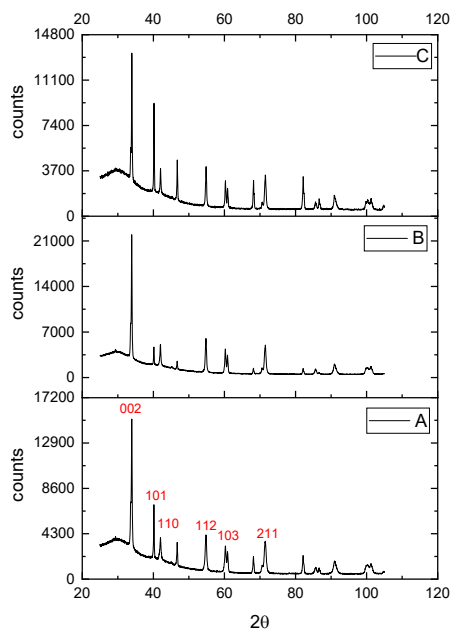


Figure 3. XRD spectra of PdO generated from the calcination of **I** (A), **II** (B) and **III** (C) complexes.

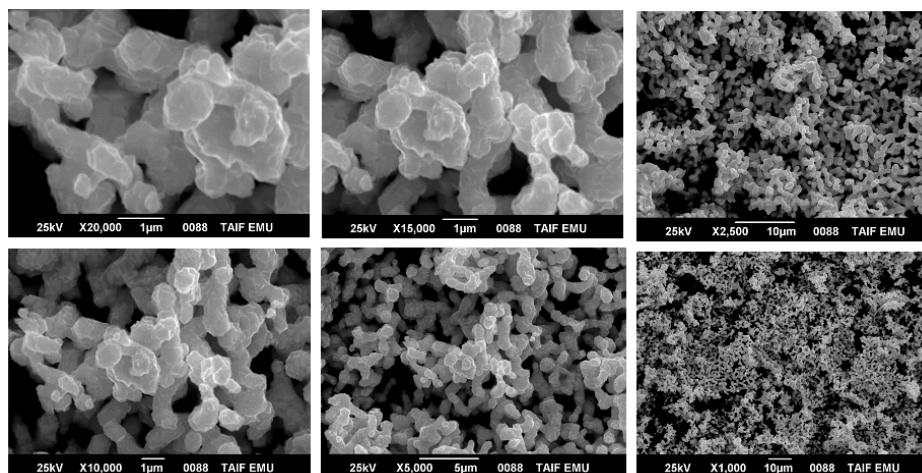


Figure 4a. SEM micrographs of PdO generated from the calcination of **I** at different magnifications.

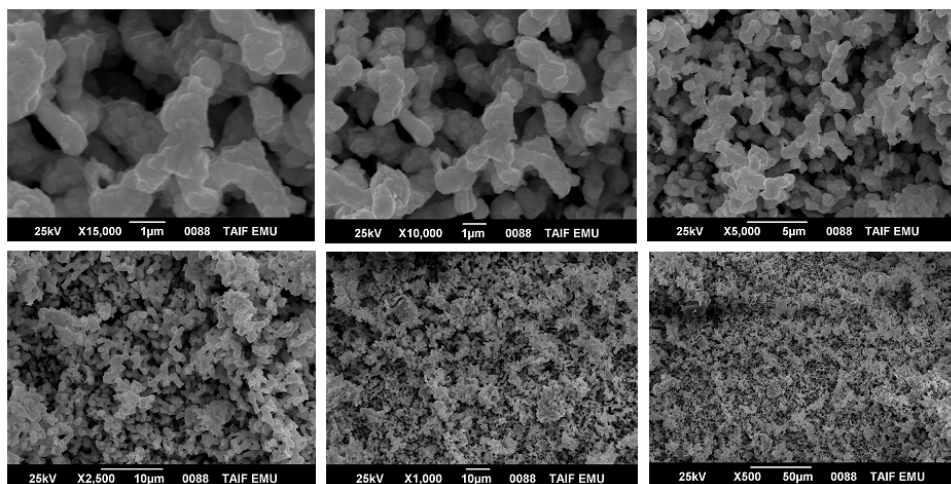


Figure 4b. SEM micrographs of PdO generated from the calcination of **II** at different magnifications.

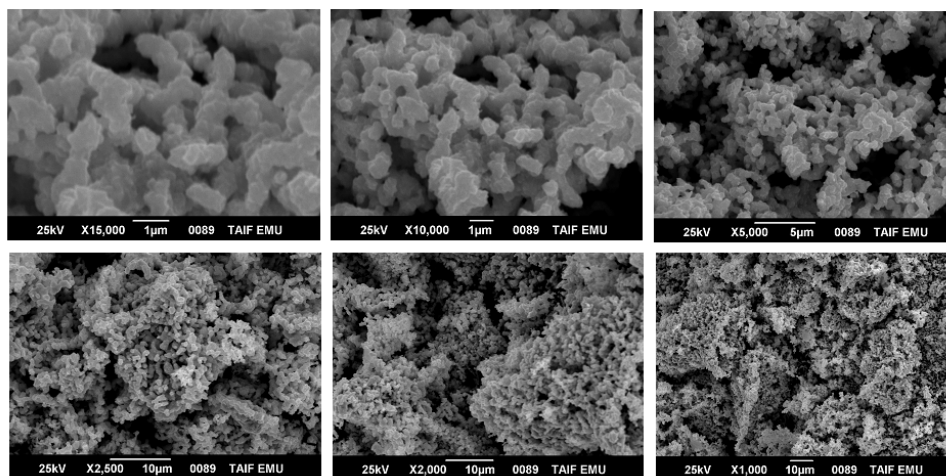


Figure 4c. SEM micrographs of PdO generated from the calcination of **III** at different magnifications.

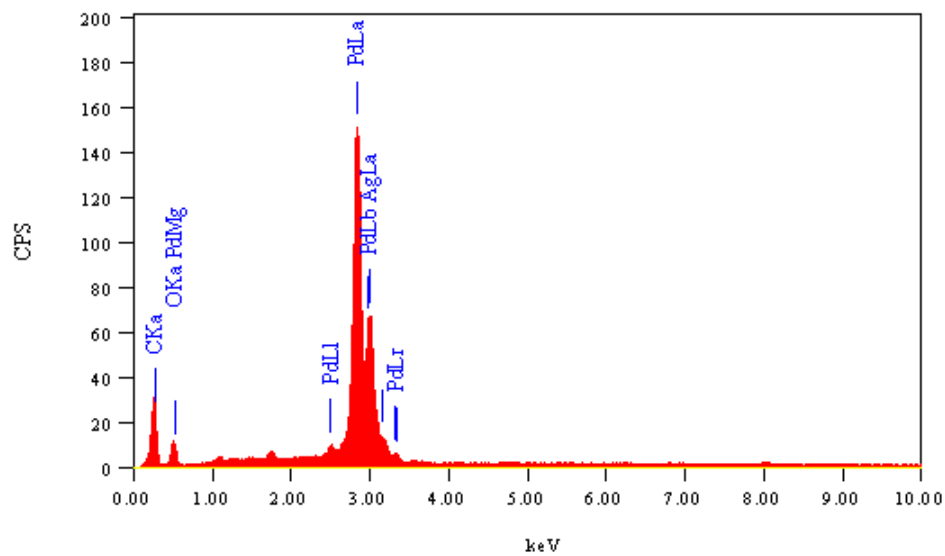


Figure 5a. EDX spectrum of PdO generated from the calcination of **I**.

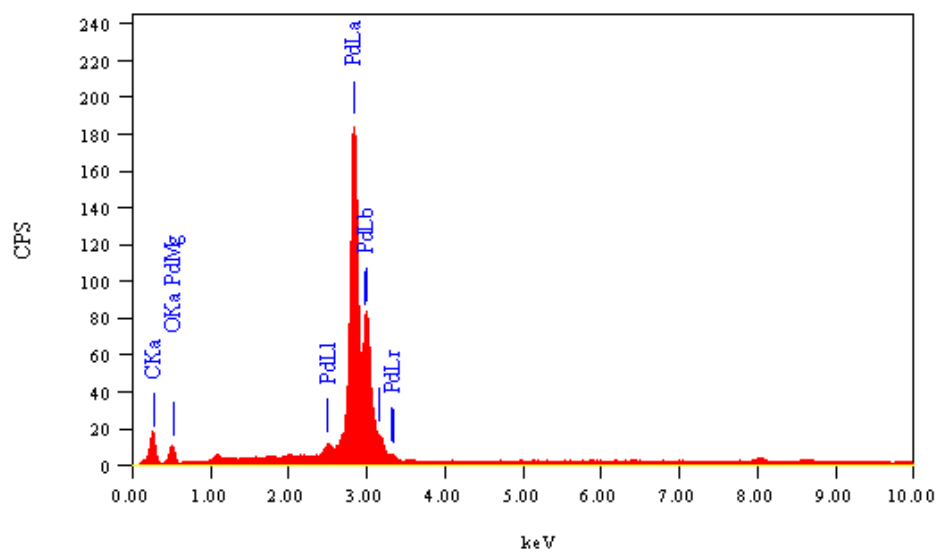


Figure 5b. EDX spectrum of PdO generated from the calcination of **II**.

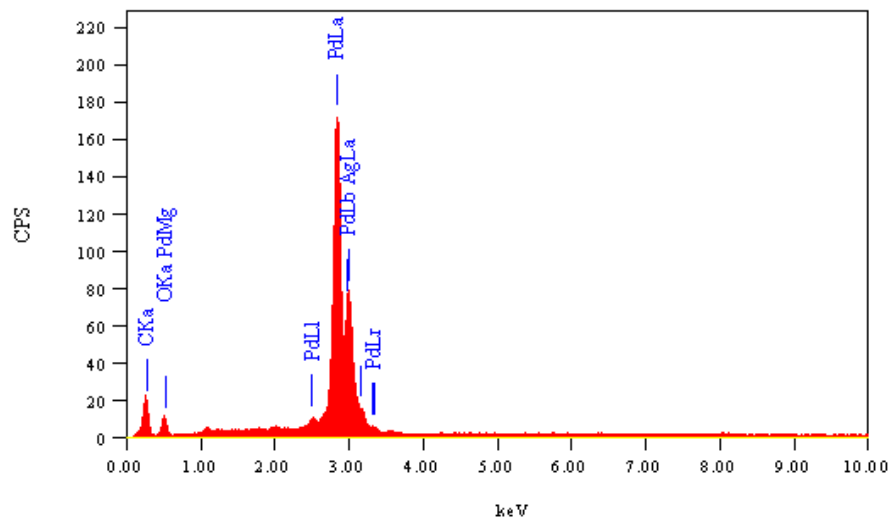


Figure 5c. EDX spectrum of PdO generated from the calcination of **III**.

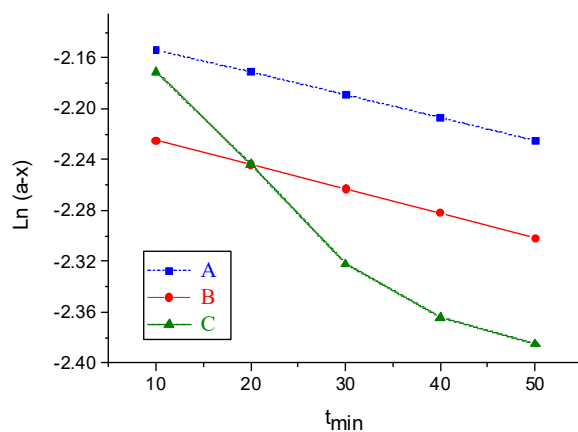


Figure 6. Effect of time (min) on the decomposition of  $\text{H}_2\text{O}_2$  using PdO prepared from the calcination of **A**; complex **I**, **B**; complex **II**, and **C**; complex **III**.

Elemental analysis of the prepared PdO materials has been verified using the EDX technique, and their EDX spectra are illustrated in Figure 5 a-c. These spectra confirmed the successful preparation of the PdO products by the formation of the major emission energies of palladium and oxygen peaks.

*Catalytic activity of the PdO materials*

Table 1 lists the catalytic activity data for the decomposition of H<sub>2</sub>O<sub>2</sub> at a constant weight of PdO and a constant concentration of H<sub>2</sub>O<sub>2</sub> (0.01 N) at room temperature. Figure 6 shows that the rate of decomposition of H<sub>2</sub>O<sub>2</sub> increased with time, which after 50 min were  $1.8 \times 10^{-3} < 2.0 \times 10^{-3} < 7.8 \times 10^{-3}$  for the synthesized PdO products from the thermal decomposition of **I**, **II** and **III**, respectively. The catalytic decomposition of H<sub>2</sub>O<sub>2</sub> tends to be associated with an intermediate radical species, which can bind to the surfaces where H<sub>2</sub>O<sub>2</sub> undergoes decomposition [44, 45]. The degree of decomposition of H<sub>2</sub>O<sub>2</sub> showed inverse dependent on the surface area, pore volume and mean pore dimensions. The chemical nature of the surface, rather than the porosity characterizations, was the principal factor in enhancing the disproportionation of H<sub>2</sub>O<sub>2</sub> on the prepared PdO oxides.

Table 1. Catalytic activity data of the PdO synthesized from the calcination of **I**, **II** and **III**.

PdO synthesized from calcination of <b>I</b>					
Results	t <sub>min</sub>				
	10	20	30	40	50
V <sub>(KMnO4)</sub>	5.8	5.7	5.6	5.5	5.4
N <sub>(H2O2) a-x</sub>	0.116	0.114	0.112	0.110	0.108
Ln(a-x)	-2.154	-2.171	-2.189	-2.207	-2.225
K	1.8 × 10 <sup>-3</sup>				
PdO synthesized from calcination of <b>II</b>					
V <sub>(KMnO4)</sub>	5.4	5.3	5.2	5.1	5.0
N <sub>(H2O2) a-x</sub>	0.108	0.106	0.104	0.102	0.100
Ln(a-x)	-2.225	-2.244	-2.263	-2.282	-2.302
K	2.0 × 10 <sup>-3</sup>				
PdO synthesized from calcination of <b>III</b>					
V <sub>(KMnO4)</sub>	5.7	5.3	4.9	4.7	4.6
N <sub>(H2O2) a-x</sub>	0.114	0.106	0.098	0.094	0.092
Ln(a-x)	-2.171	-2.244	-2.322	-2.364	-2.385
K	7.8 × 10 <sup>-3</sup>				

\*K (min<sup>-1</sup>) = rate constant of the H<sub>2</sub>O<sub>2</sub> decomposition.

**CONCLUSION**

In this work, nanostructured PdO oxide nanomaterials were synthesized by the calcination of three Pd(II) complexes. These complexes contained ofloxacin drug, amino acid (alanine or glycine), and Pd(II) ions. The structure and morphology of the synthesized PdO nanomaterials were characterized using FTIR, XRD, SEM, and EDX techniques. The PdO nano oxides were tested as a catalyst for the heterogeneous catalytic activity degradation of H<sub>2</sub>O<sub>2</sub> solution at room temperature.

**ACKNOWLEDGEMENT**

The authors extend their appreciation to the Deputyship for Research & Innovation, Ministry of Education in Saudi Arabia for funding this research work through the project number 127-441-1.

## REFERENCES

1. Garey, K.W.; Amsden, G.W. Trovafloxacin: An overview. *Pharmacotherapy* **1999**, *19*, 21-34.
2. Fitton, A. The quinolones. *Clin Pharmacokinet.* **1992**, *22* (suppl 1), 1-11.
3. Stein, G.E. Pharmacokinetics and pharmacodynamics of newer fluoroquinolones. *Clin Infect. Dis.* **1996**, *23* (suppl 1), S19-S24.
4. Norrby, S.R.; Lietman, P.S. Safety and tolerability of fluoroquinolones. *Drugs* **1993**, *45* (suppl 3), 59-64.
5. King, D.E.; Malone, R.; Lilley, S.H. New classification and update on the quinolone antibiotics. *Am. Fam. Physician.* **2000**, *61*, 2741-2748.
6. Ruiz, M.; Ortiz, R.; Perello, L. Ni(II) and Zn(II) complexes with cinoxacin. Synthesis and characterization of  $M(Cx)_2(DMSO)_n(H_2O)_m$  ( $n = 0, 2; m = 2, 4$ ). Crystal structures of  $[M(Cx)_2(DMSO)_2] \cdot 4H_2O$  ( $M = Ni(II), Zn(II)$ ). *Inorg. Chim. Acta* **1993**, *211*, 133-139.
7. Ruiz, M.; Ortiz, R.; Perello, L.; Garcia-Granda, S.; Diaz, M.R. Synthesis and characterization of Cd(II) complexes of cinoxacin. Crystal structure of a dicadmium complex containing two monoatomic-bridging carboxylate oxygen atoms. *Inorg. Chim. Acta.* **1994**, *217*, 149-154.
8. Huang, G.-M.; Tsai, T.-C.; Huang, C.-W.; Kumar, N.; Tseng, T.-Y.; Wu, W.-W. Dynamic observation of reversible lithium storage phenomena in hybrid supercapacitor devices. *Nano Energy*, **2017**, *41*, 494-500.
9. Ren, H.; Yu, R.; Qi, J.; Zhang, L.; Jin, Q.; Wang, D. Hollow Multishelled Heterostructured Anatase/TiO<sub>2</sub>(B) with Superior Rate Capability and Cycling Performance. *Adv. Mater.* **2019**, *31*(10), 1805754.
10. Li, Y.F.; Shi, Y.H.; Wang, S.G.; Liu, J.H.; Lin, J.; Xia, Y.; Wu, X.L.; Fan, C.Y. Carbon/Binder-Free NiO@NiO/NF with In Situ Formed Interlayer for High-Areal-Capacity Lithium Storage. *Adv. Eng. Mater.* **2019**, 1803690.
11. Bencheikh, Y.; Harnois, M.; Jijie, R.; Addad, A.; Roussel, P.; Szuneris, S.; Hadjersi, T.; Boukherroub, R. High performance silicon nanowires/ruthenium nanoparticles micro-supercapacitors. *Electrochim. Acta.* **2019**, *311*, 150-159.
12. Zhang, Y.; Park, S.-J. Incorporation of RuO<sub>2</sub> into charcoal-derived carbon with controllable microporosity by CO<sub>2</sub> activation for high-performance supercapacitor. *Carbon*, **2017**, *122*, 287-297.
13. Fu, Y.; Gao, X.; Zha, D.; Zhu, J.; Ouyang, X.; Wang, X. Yolk-shell-structured MnO<sub>2</sub> microspheres with oxygen vacancies for high-performance supercapacitors. *J. Mater. Chem.* **2018**, *6*, 1601-1611.
14. Asim, S.; Javed, M.S.; Hussain, S.; Rana, M.; Iram, F.; Lv, D.; Hashim, M.; Saleem, M.; Khalid, M.; Jawaria, R.; Ullah, Z.; Gull, N. RuO<sub>2</sub> nanorods decorated CNTs grown carbon cloth as a free-standing electrode for supercapacitor and lithium ion batteries. *Electrochim. Acta.* **2019**, *326*, 135009. <https://doi.org/10.1016/j.electacta.2019.135009>
15. Ruiz, M.; Perello, L.; Ortiz, R.; Castineiras, A.; Maichle-Mossmar, C.; Canton, E. Synthesis, characterization, and crystal structure of  $[Cu(cinoxacinate)_2] \cdot 2H_2O$  complex: A square-planar CuO<sub>4</sub> chromophore. Antibacterial studies. *J. Inorg. Biochem.* **1995**, *59*, 801-810.
16. Ruiz, M.; Ortiz, R.; Perello, L.; Latorre, J.; Server-Carrio, J. Potentiometric and spectroscopic studies of transition-metal ions complexes with a quinolone derivative (cinoxacin). Crystal structures of new Cu(II) and Ni(II) cinoxacin complexes. *J. Inorg. Biochem.* **1997**, *65*, 87-96.
17. Ruiz, M.; Perello, L.; Server-Carrio, J.; Ortiz, R.; Garcia-Granda, S.; Diaz, M.R.; Canton, E. Cinoxacin complexes with divalent metal ions. Spectroscopic characterization. Crystal structure of a new dinuclear Cd(II) complex having two chelate-bridging carboxylate groups. Antibacterial studies. *J. Inorg. Biochem.* **1998**, *69*, 231-239.

18. Macias, B.; Villa, M.V.; Rubio, I.; Castineiras, A.; Borrás, J. Synthesis, characterization, and crystal structure of  $[\text{Cu}(\text{cinoxacinate})_2] \cdot 2\text{H}_2\text{O}$  complex: A square-planar  $\text{CuO}_4$  chromophore. Antibacterial studies. *J. Inorg. Biochem.* **1995**, *59*, 801-810.
19. Li, Y.H.; Tang, Y.Z.; Huang, X.F.; Xiong, R.G. The Crystal Structure of a Gatifloxacin Complex and its Fluorescent Property. *Z. Anorg. Allg. Chem.* **2005**, 631, 639-641.
20. Psomas, G.; Tarushi, A.; Efthimiadou, E.K.; Sanakis, Y.; Raptopoulou, C.P.; Katsaros, N. Synthesis, structure and biological activity of copper(II) complexes with oxolinic acid. *J. Inorg. Biochem.* **2006**, *100*, 1764-1773.
21. Sunberg, R.J.; Martin, R.B. Interactions of histidine and other imidazole derivatives with transition metal ions in chemical and biological systems. *Chem. Rev.* **1974**, *74*, 471-517.
22. Nagaraja, R.; Nagappa, B.; Girija, C.R.; Nagabhushana, B.M. Synthesis and Characterization of Nanocrystalline MgO Powder and its Application in the Treatment of Pharmaceutical Effluent. *J. Nanotech. Appl.* **2011**, *11*, 28.
23. Cheng, I.; Wang, J.; Tsai, C.; Chen, Y.; Pan, F. Correlation of surface processes with characteristic sensing responses of PdO thin films to ethanol. *Appl. Surf. Sci.* **2019**, *473*, 589-596.
24. Huang, C.-J.; Pan, F.-M.; Chen, H.-Y.; Chang, L. Growth and photoresponse study of PdO nanoflakes reactive-sputter deposited on  $\text{SiO}_2$ . *J. Appl. Phys.* **2010**, *108*, 053105.
25. Veziroglu, S.; Hwang, J.; Drewes, J.; Barg, I.; Shondo, J.; Strunskus, T.; Polonskyi, O.; Faupel, F.; Aktas, O.C. PdO nanoparticles decorated  $\text{TiO}_2$  film with enhanced photocatalytic and self-cleaning properties. *Mater. Today Chem.* **2020**, *16*, 100251. <https://doi.org/10.1016/j.mtchem.2020.100251>
26. Hadi, A.; Yaacob, I.I. Synthesis of PdO/CeO<sub>2</sub> mixed oxides catalyst for automotive exhaust emissions control. *Catal. Today* **2004**, *96*, 165-170.
27. Khojasteh, H.; Salavati-Niasari, M.; Abbasi, A.; Azizi, F.; Enhessari, M. Synthesis, characterization and photocatalytic activity of PdO/ $\text{TiO}_2$  and Pd/ $\text{TiO}_2$  nanocomposites. *J. Mater. Sci. Mater. Electron.* **2016**, *27*, 1261-1269.
28. Zhou, W.; Guan, Y.; Wang, D.; Zhang, X.; Liu, D.; Jiang, H.; Wang, J.; Liu, X.; Liu, H. PdO/ $\text{TiO}_2$  and Pd/ $\text{TiO}_2$  Heterostructured Nanobelts with Enhanced Photocatalytic Activity. *Chem. Asian J.* **2014**, *9*, 1648-1654.
29. Ismail, A.A. Mesoporous PdO– $\text{TiO}_2$  nanocomposites with enhanced photocatalytic activity. *Appl. Catal. B Environ.* **2012**, *117-118*, 67-72.
30. Huang, C.-J.; Pan, F.-M.; Chang, I.-C. Enhanced photocatalytic decomposition of methylene blue by the heterostructure of PdO nanoflakes and  $\text{TiO}_2$  nanoparticles. *Appl. Surf. Sci.* **2012**, *263*, 345-351.
31. Letichevsky, S.; Zonetti, P.C.; Reis, P.P.P.; Celnik, J.; Rabello, C.R.K.; Gaspar, A.B.; Appel, L.G. The role of *m*- $\text{ZrO}_2$  in the selective oxidation of ethanol to acetic acid employing PdO/*m*- $\text{ZrO}_2$ . *J. Mol. Catal. A Chem.* **2015**, *410*, 177-183.
32. Reis, P.P.P.; Zonetti, P.C.; Passos, F.B.; Appel, L.G. Acetic Acid Synthesis from Ethanol: Describing the Synergy Between PdO and *m*- $\text{ZrO}_2$ . *Catal. Lett.* **2017**, *147*, 821-827.
33. Jürgensen, A.; Heutz, N.; Raschke, H.; Merz, K.; Hergenröder, R. Behavior of Supported Palladium Oxide Nanoparticles under Reaction Conditions, Studied with near Ambient Pressure XPS. *Anal. Chem.* **2015**, *87*, 7848-7856.
34. Dogra, V.; Kaur, G.; Kumar, R.; Kumar, S. Toxicity assessment of palladium oxide nanoparticles derived from metallosurfactants using multi assay techniques in *Allium sativum*. *Colloids Surf. B.* **2020**, *187*, 110752.
35. Das, P.; Linert, W. Schiff base-derived homogeneous and heterogeneous palladium catalysts for the Suzuki–Miyaura reaction. *Coord. Chem. Rev.* **2016**, *311*, 1-23.
36. Saldan, I.; Semenyuk, Y.; Marchuk, I.; Reshetnyak, O. Chemical synthesis and application of palladium nanoparticles. *J. Mater. Sci.* **2015**, *50*, 2337-2354.

37. Sheldon, R.A. Recent advances in green catalytic oxidations of alcohols in aqueous media. *Catal. Today*. **2015**, 247, 4-13.
38. Aditya, T.; Pal, A.; Pal, T. Nitroarene reduction: a trusted model reaction to test nanoparticle catalysts. *Chem. Commun.* **2015**, 51, 9410-9431.
39. Pramanik, S.; Das, M.R.; Das, D.; Das, P. Sustainable Redox Chemistry Route to Multifaceted Fe-Pd Heteronanostructure: Delving into the Synergistic Influence in Catalysis. *ChemistrySelect*. **2017**, 2, 4577-4585.
40. Naglah, A.M.; Al-Omar, M.A.; Almhizia, A.A.; AlKahtani, H.M.; Bhat, M.A.; Al-Shakliah, N.S.; Belgacem, K.; Majrashi, B.M. Refat, M.S.; Adam, A.M.A. Synthesis, thermogravimetric, and spectroscopic characterizations of three palladium metal(II) ofloxacin drug and amino acids mixed ligand complexes as advanced antimicrobial materials. *J Mol. Struct.* **2021**, 1225, article No. 129102 pages 1-10.
41. Rao, C.N.R. *Chemical Applications of Infrared spectroscopy*, Academic Press, New York, and London, **1963**.
42. Wang, Y.; Herron, N. Nanometer-sized semiconductor clusters: materials synthesis, quantum size effects, and photophysical properties. *J. Phys. Chem.* **1991**, 95, 525-532.
43. He, H.; Gao, C. A General Strategy for the Preparation of Carbon Nanotubes and Graphene Oxide Decorated with PdO Nanoparticles in Water. *Molecules*. **2010**, 15, 4679-4694.
44. Lousada, C.M.; Jonsson, M. Kinetics, Mechanism, and Activation Energy of H<sub>2</sub>O<sub>2</sub> Decomposition on the Surface of ZrO<sub>2</sub>. *J. Phys. Chem.* **2010**, 114, 11202-11208.
45. Zigah, D.; Lopez, J.R.; Bard, A. Quantification of photoelectrogenerated hydroxyl radical on TiO<sub>2</sub> by surface interrogation scanning electrochemical microscopy. *J. Phys. Chem.* **2012**, 14, 12764-12772.